

AperTO - Archivio Istituzionale Open Access dell'Università di Torino

**From biowaste to magnet-responsive materials for water remediation from polycyclic aromatic hydrocarbons**

**This is the author's manuscript**

*Original Citation:*

*Availability:*

This version is available <http://hdl.handle.net/2318/1665938> since 2019-01-16T12:10:04Z

*Published version:*

DOI:10.1016/j.chemosphere.2018.03.153

*Terms of use:*

Open Access

Anyone can freely access the full text of works made available as "Open Access". Works made available under a Creative Commons license can be used according to the terms and conditions of said license. Use of all other works requires consent of the right holder (author or publisher) if not exempted from copyright protection by the applicable law.

(Article begins on next page)

# Accepted Manuscript

From biowaste to magnet-responsive materials for water remediation from polycyclic aromatic hydrocarbons

Roberto Nisticò, Federico Cesano, Flavia Franzoso, Giuliana Magnacca, Domenica Scarano, Israel G. Funes, Luciano Carlos, Maria E. Parolo



PII: S0045-6535(18)30576-9

DOI: [10.1016/j.chemosphere.2018.03.153](https://doi.org/10.1016/j.chemosphere.2018.03.153)

Reference: CHEM 21097

To appear in: *ECSN*

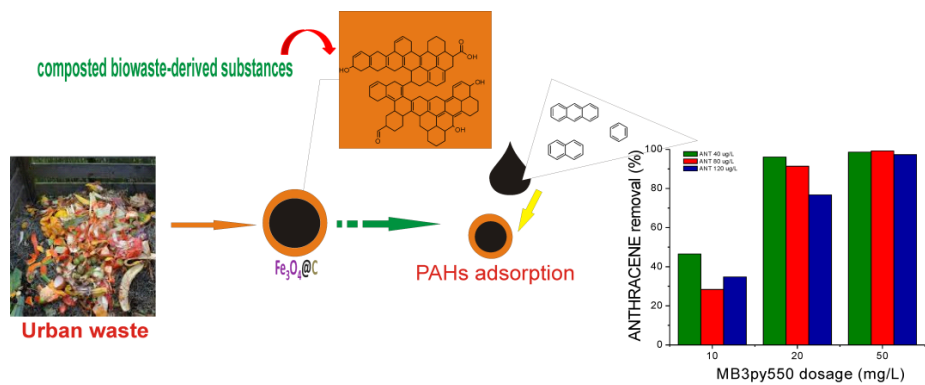
Received Date: 25 January 2018

Revised Date: 21 March 2018

Accepted Date: 22 March 2018

Please cite this article as: Nisticò, R., Cesano, F., Franzoso, F., Magnacca, G., Scarano, D., Funes, I.G., Carlos, L., Parolo, M.E., From biowaste to magnet-responsive materials for water remediation from polycyclic aromatic hydrocarbons, *Chemosphere* (2018), doi: 10.1016/j.chemosphere.2018.03.153.

This is a PDF file of an unedited manuscript that has been accepted for publication. As a service to our customers we are providing this early version of the manuscript. The manuscript will undergo copyediting, typesetting, and review of the resulting proof before it is published in its final form. Please note that during the production process errors may be discovered which could affect the content, and all legal disclaimers that apply to the journal pertain.



# 1 From biowaste to magnet-responsive materials for water remediation from polycyclic 2 aromatic hydrocarbons

3  
4 Roberto Nisticò<sup>a,b,‡</sup>, Federico Cesano<sup>a,c,‡</sup>, Flavia Franzoso<sup>a</sup>, Giuliana Magnacca<sup>a,c</sup>, Domenica  
5 Scarano<sup>a,c</sup>, Israel G. Funes<sup>d</sup>, Luciano Carlos<sup>e</sup>, Maria E. Parolo<sup>d,\*</sup>

6  
7 <sup>a</sup>University of Torino, Department of Chemistry, Via P. Giuria 7, 10125 Torino, Italy.

8 <sup>b</sup>Polytechnic of Torino, Department of Applied Science and Technology DISAT, C.so Duca degli Abruzzi 24, 10129  
9 Torino, Italy.

10 <sup>c</sup>NIS Interdepartment Centre, Via P. Giuria 7, 10125 Torino, Italy.

11 <sup>d</sup>Instituto de Investigación en Toxicología Ambiental y Agrobiotecnología, CITAAC (CONICET-UNCo), Facultad de  
12 Ingeniería, Universidad Nacional Del Comahue, Buenos Aires 1400, 8300 Neuquén, Argentina.

13 <sup>e</sup>Instituto de Investigación y Desarrollo en Ingeniería de Procesos, Biotecnología y Energías Alternativas, PROBIEN  
14 (CONICET-UNCo), Facultad de Ingeniería, Universidad Nacional Del Comahue, Buenos Aires 1400, 8300 Neuquén,  
15 Argentina.

16 <sup>‡</sup> Both authors contributed equally to this work.

17 \* Corresponding author. E-mail: maria.parolo@fain.uncoma.edu.ar, Ph.: +54 299 4490300 x 678 , Fax: +54 299  
18 4490329

## 19 20 **Abstract**

21 Composted urban biowaste-derived substances (BBS-GC) are used as carbon sources for the  
22 preparation of carbon-coated magnet-sensitive nanoparticles obtained via co-precipitation method  
23 and the subsequent thermal treatment at 550 °C under nitrogen atmosphere. A multitechnique  
24 approach has been applied to investigate the morphology, magnetic properties, phase composition,  
25 thermal stability of the obtained magnet-sensitive materials. In particular, pyrolysis-induced  
26 modifications affecting the BBS-GC/carbon shell were highlighted. The adsorption capacity of such  
27 bio-derivative magnetic materials for the removal of hydrophobic contaminants such as polycyclic  
28 aromatic hydrocarbons was evaluated in order to verify their potential application in wastewater  
29 remediation process. The promising results suggest their use as a new generation of magnet-  
30 responsive easily-recoverable adsorbents for water purification treatments.

31  
32 **Keywords:** Adsorption; Biomass valorization; Iron oxides; Magnetic nanomaterials; Pyrolysis.

## 33 34 **1. Introduction**

35 In recent years, a wide number of studies has been dedicated to the valorization of biowaste and  
36 biowaste-derived substances in order to prepare novel smart products, thus reaching a reduction of  
37 the industrial and/or urban residues, re-entering them in the economic cycle in a more sustainable  
38 and environmental-friendly development of our society (Fava et al., 2015; G. Magnacca et al.,  
39 2015; Deng et al., 2016; Nisticò, 2017a). In particular, low-cost starting materials from natural  
40 sources (i.e., clays and minerals as well as biopolymers), industrial wastes and agriculture residues  
41 (such as lignin and humic/fulvic acid-like substances, chitin and chitosan, alginate and waste  
42 slurry), are considered as an important source of fine chemicals in substitution of the more  
43 traditional petroleum-derived ones (Bailey et al., 1999; Avetta et al., 2014; Vakili et al., 2014;  
44 Bautista et al., 2015; Choi et al., 2015a; Choi et al., 2015b; Manna et al., 2015; Nisticò et al., 2015;  
45 Franzoso et al., 2016). Among these low-cost bio-based sources, lignocellulose-derived materials  
46 and chitin/chitosan seem to be highly attractive resources for the future generation of chemicals  
47 (Tran et al., 2015).

48 Shape- and size-controlled smart magnetic nanoparticles (mNPs) consisting in a magnet-sensitive  
49 core made of iron oxides (i.e., magnetite/maghemite) stabilized by one or more covering layer(s),  
50 currently attracted the interests of worldwide experts due to their unique magnet-responsive  
51 properties which favor their uses in several technological applications, such as drug-delivery or  
52 contaminated wastewater (bio)remediation processes (Cesano et al., 2016; Lata and Samadder,  
53 2016; Zhao et al., 2016; Lu et al., 2007; Nisticò, 2017b). In this context, various protective and/or  
54 stabilizing materials were investigated for inducing particular surface properties at the mNPs.  
55 Typically, both oxides (mainly silica) and/or organic (surfactants, (bio)polymers, and carbons)  
56 coatings were considered as possible covering-materials, thus combining the advantages of both  
57 components selected (namely, the magnet-sensitive Fe-containing oxides core and the functionality  
58 at the surface) (Lu et al., 2007; Li et al., 2013; Nardi et al., 2013).

59 As already evidenced in our previous works (Nisticò et al., 2015; Franzoso et al., 2017; Nisticò et  
60 al., 2018), Bio-Based Substances (BBS-GC, where GC stands for green compost) are  
61 supramolecular aggregates made of organic macromolecules with a highly branched and complex  
62 lignin-derived structure. Such substances are isolated from urban composted biowastes after more  
63 than 180 days of composting, and as a consequence of the starting material complexity (i.e., urban  
64 public park trimming and home gardening residues), BBS-GC contain several functional groups  
65 (the BBS-GC chemical structure and functionalities are fully reported in **Table S1**, whereas their  
66 thermal stability is reported in **Figure S1**) (Nisticò et al., 2015). The macromolecular nature of  
67 these BBS, very similar to humic/fulvic substances with several O-containing functional groups,  
68 suggested their potential use as stabilizing/protective agents for the greener synthesis of mNPs with  
69 both adsorption properties and enhanced photoactive response in advanced oxidation processes  
70 (AOPs) for the remediation of contaminated water (Magnacca et al., 2014).

71 Polycyclic aromatic hydrocarbons (PAHs) are among the most ubiquitous environmental  
72 contaminants (Vane et al., 2013). Due to their resistance to biodegradation and bioaccumulation, the  
73 presence of the PAHs in surface water, groundwater, and drinking water, poses a major risk to  
74 human health and wildlife. Different techniques have been developed for removing PAHs from  
75 contaminated water, among which physical remediation by means of selective adsorbents is one of  
76 the most frequently used strategies due to its high effectiveness and low operational cost (Pérez et  
77 al., 2008; Dave and Ghaly, 2011).

78 Conventional adsorbents selected for their high oleophilic properties in contaminated water  
79 remediation are polymeric foams in the shape of rolls and/or sheets (typically made of  
80 polypropylene, polystyrene, and polyurethane) (Teas et al., 2001; Dave and Ghaly, 2011).  
81 Additionally, as reported in the literature, high-surface-area activated carbons and graphitic carbons  
82 can be a very interesting alternative as adsorbents in wastewater treatments (Lee et al., 2006;  
83 Cesano et al., 2012; Magnacca et al., 2018 ). Hu et al. (2014) demonstrated the use of compressible

84 carbon nanotube-graphene hybrid aerogels having hydrophobicity and oleophilicity for oil sorption.  
85 However, the use of such materials, especially in open-space contaminated areas, presents some  
86 limitations, one above all the difficulties in their recovering. Therefore, a step forward in this field  
87 is the preparation of easily-recoverable carbon-coated magnet-sensitive materials (Wang et al.,  
88 2006; Lu et al., 2007; Hao et al., 2014; Cesano et al., 2016).

89 Magnetic materials consisting of iron oxides (i.e magnetite/maghemite) particles stabilized by  
90 functional carbon shells, received a great attention as easily-recoverable magnet-responsive smart  
91 materials for wastewater remediation (Hao et al., 2014; Mehta et al., 2015). Recently, in our  
92 previous study (Nisticò et al., 2017), another biowaste-derived substrate (namely, chitosan) was  
93 selected as starting material for the preparation of carbon-coated magnet-sensitive composite  
94 materials for water remediation from PAHs, with promising results.

95 Therefore, the aim of this study is the preparation and physicochemical characterization of carbon-  
96 coated magnetite/maghemite NPs synthesized through iron salts co-precipitation process in the  
97 presence of BBS as initial stabilizers and carbon-source. Pyrolysis under nitrogen atmosphere is  
98 carried out at mild condition (550 °C), in order to convert the BBS into a carbon layer without  
99 altering the structure and properties of magnetite. Morphology, thermal stability and magnetic  
100 properties of such composites mNPs were fully assessed. Adsorption experiments involving the  
101 water remediation from a PAHs mixture by direct contact with such BBS-derived carbon-materials  
102 and subsequent easily-recovery by magnetic separation are also examined.

103

## 104 **2. Material and methods**

### 105 **2.1 Materials**

106 Anhydrous ferric chloride  $\text{FeCl}_3$  (CAS 7705-08-0, purity  $\geq 98\%$ , Fluka Chemika) and ferrous  
107 sulphate heptahydrate  $\text{FeSO}_4 \cdot 7\text{H}_2\text{O}$  (CAS 7782-63-0, purity  $\geq 99.5\%$ , Fluka Chemika) were  
108 selected as iron oxide precursors. Bio-Based Substances (BBS-GC) were obtained following a

109 previously reported procedure (Nisticò et al., 2015) starting from urban composted biowastes (i.e.,  
110 urban public park trimming and home gardening residues after 180 days of composting) sampled  
111 from the process lines of *ACEA Pinerolese Industriale S.p.A.* waste treatment plant in Pinerolo  
112 (Italy) in an advanced system that comprises specific technological facilities, developed by *ACEA*  
113 *Pinerolese Industriale S.p.A.* and under European validation. Naphthalene (NAP;  $\log K_{ow} = 3.37$ ),  
114 acenaphthene (AC;  $\log K_{ow} = 3.98$ ), acenaphthylene (ACL;  $\log K_{ow} = 4.07$ ), fluorine (FL;  $\log K_{ow} =$   
115 4.18), anthracene (ANT;  $\log K_{ow} = 4.46$ ), phenanthrene (PHE;  $\log K_{ow} = 4.50$ ), pyrene (PY;  $\log K_{ow} =$   
116 4.88) and fluoranthene (FN;  $\log K_{ow} = 4.90$ ) were purchased from Sigma-Aldrich (purity > 99.0%).  
117 The aqueous solutions for adsorption experiments were prepared using ultrapure water Millipore  
118 Milli-Q™ and all chemicals were used without further purification.

119

## 120 2.2 Preparation of BBS-derived carbon magnet-sensitive materials

121 The starting BBS-stabilized magnetite NPs were synthesized following the procedure reported in  
122 the literature (Franzoso et al., 2017; Nisticò et al., 2018). In detail, 3.7 g of  $\text{FeCl}_3$  and 4.17 g of  
123  $\text{FeSO}_4 \cdot 7\text{H}_2\text{O}$  (molar ratio  $\text{Fe(III)/Fe(II)} = 1.5$ ) were dissolved in 100 mL of deionized water and  
124 heated up to 90 °C. Once the temperature was reached, two solutions were added in sequence: a) 10  
125 mL of 25 vol.% ammonium hydroxide, and b) 50 mL of a previously prepared BBS aqueous  
126 solution. Three solutions with different content of BBS were employed: 1, 2, and 3 wt.%,  
127 respectively. The mixture was mechanically stirred at 90 °C for 30 min and then cooled down to  
128 room temperature (RT). Such dispersions of BBS-stabilized magnetite NPs were purified by  
129 washing twice with deionized water, deposited onto glass Petri dishes, and oven-dried at 80 °C  
130 overnight. BBS-derived magnetic-materials were then thermally treated in a quartz tube under  
131 nitrogen atmosphere ( $\text{N}_2$  flux of  $250 \text{ mL min}^{-1}$ ) for 1 h at 550 °C (from RT to the target  
132 temperature, heating ramp  $5 \text{ °C min}^{-1}$ ). The resulting materials were manually crumbled in a mortar  
133 for the further experiments. In analogy to our previous work (Franzoso et al., 2017), depending on



134 the different BBS amount (1, 2 and 3 wt.%), the obtained NPs were coded with the acronym MB1,  
135 MB2 and MB3, respectively. Thermally-treated samples were further coded with pyT, where py  
136 stands for pyrolysis, and T refers to the temperature of pyrolysis (550 °C). Magnetite (M0), as  
137 obtained following the co-precipitation procedure without the BBS addition, was taken as a neat  
138 magnetite/maghemite reference.

139

### 140 **2.3 Physicochemical characterization**

141 Scanning electron microscopy (SEM) analyses were carried out by using a ZEISS EVO 50 XVP  
142 microscope with LaB<sub>6</sub> source, equipped with detectors for secondary electron collection and energy  
143 dispersive X-ray Spectroscopy (EDS). SEM micrographs were obtained after sputtering samples  
144 with a 10-15 nm thick gold film. Atomic force microscopy (AFM) and magnetic force microscopy  
145 (MFM) measurements were performed by using a modified Nanosurf Easyscan2 AFM instrument,  
146 equipped with a 10 μm scan-head, high performance anti-vibration platform in an acoustically  
147 insulated enclosure and Faraday cage. AFM and MFM images were obtained in a dual-pass mode:  
148 the first scan was for the morphological imaging in the intermittent contact mode, while the second  
149 scan was operated at constant-height (H) above the same surface with a magnetic probe (Multi75M-  
150 G, Budget Sensors; resonant frequency = 75 kHz, force constant = 3 N m<sup>-1</sup>) having a tip radius of  
151 about 60 nm by monitoring the shifting of the phase and of the amplitude signals. The magnetic tip  
152 was magnetized by an external magnet (magnetization along the tip-axis) and tested on a magnetic  
153 grid prior to measurements. Magnetization measurements were carried out performing experiments  
154 in a LakeShore 7404 vibrating sample magnetometer. The hysteresis loop of the samples was  
155 registered at RT cycling the magnetic field from -20000 to 20000 Oe. X-ray diffraction (XRD)  
156 patterns were obtained by using an X'Pert PRO MPD diffractometer from PANalytical, equipped  
157 with Cu anode, working at 40 kV and 30 mA, with a Bragg-Brentano geometry, in a flat sample-  
158 holder. The acquisition was performed in a 0.02° interval steps, with 45 s step<sup>-1</sup>. Fourier transform

159 infrared (FTIR) spectra were registered in transmission mode using a Bruker Vector 22  
160 spectrophotometer equipped with Globar source, DTGS detector, and working with 128 scans at 4  
161  $\text{cm}^{-1}$  resolution in the 4000-400  $\text{cm}^{-1}$  range. Samples were analyzed as self-supporting pellets by  
162 dispersing the mNPs in KBr (1:20 weight ratio).

163

## 164 **2.4 Adsorption experiments**

165 **2.4.1 Single component PAH system:** preliminary adsorption experiments were performed using  
166 ANT as reference PAH substrate. Kinetic experiments were carried out contacting the adsorbent  
167 ( $500 \text{ mg L}^{-1}$ ) with an ANT solution ( $50 \text{ } \mu\text{g L}^{-1}$ ) at pH 6 and sampling at fixed times up to a  
168 maximum of 24 hours. After contact, an aliquot of 5 mL was recovered, the solid magnetically  
169 separated from the solution and the supernatant analyzed. The effect of BBS amount contained in  
170 MB samples on adsorption phenomenon was studied considering  $[\text{ANT}] = 40 \text{ } \mu\text{g L}^{-1}$ ,  
171  $[\text{MBpy550}] = 20 \text{ mg L}^{-1}$ , Contact time = 3 hours. The ANT concentration effects on adsorption were  
172 studied at three different adsorbent dosage ( $10 \text{ mg L}^{-1}$ ,  $20 \text{ mg L}^{-1}$  and  $50 \text{ mg L}^{-1}$ ). A series of Pyrex-  
173 flasks were filled with 100 mL of ANT solutions ( $40\text{-}120 \text{ } \mu\text{g L}^{-1}$ ) and MB3py550 adsorbent were  
174 added under continuous stirring. The flasks were capped and shaken in darkness during 3 hours.  
175 After contact, an aliquot of 5 mL was recovered, the mNPs magnetically separated from the  
176 solution and the supernatant analyzed by fluorescence spectroscopy. All adsorption experiments  
177 were carried out in triplicate at  $20 \pm 1^\circ\text{C}$ . ANT concentrations were determined by fluorescence  
178 measurements obtained by means of a Hitachi F-7000 fluorescence spectrometer. The excitation  
179 wavelength selected was 250 nm, slit widths of excitation and emission were 2.5 nm, and 1 cm path  
180 length quartz cuvettes were used.

181

182 **2.4.2 Mixture of PAHs:** adsorption experiments with a mixture of eight PAHs (NAP, ACL, AC,  
183 FL, PHE, ANT, FN and PY) on MB3py550 were performed. PAHs mixture solution was prepared

184 from a dilution of PAHs mixture stock solution ( $20 \text{ mg L}^{-1}$  of each PAH in methanol) with  
185 ultrapure water and agitation during 48 h at RT in amber borosilicate glass containers. Final  
186 methanol concentrations were kept under 0.1% of the total solution volume to avoid co-solvent  
187 effects. The initial concentrations of each PAH ranged from 2.2 to  $44 \text{ } \mu\text{g L}^{-1}$ . Concentrations of  
188 each PAH after 24 h of contact with the adsorbent ( $50 \text{ mg L}^{-1}$  of MB3py550) were determined by  
189 gas chromatography mass spectrometer (GC–MS) using the following procedure: 200 mL of  
190 sample extracted after the magnetic separation was eluted through a Strata RP-18 cartridge; then,  
191 PAHs were recovered with 6 mL of dichloromethane. The fraction was concentrated to 1 mL under  
192 a nitrogen stream, transferred to a glass vial, and quantitated by GC–MS. A 30 m HP-5 MS fused  
193 silica column (0.25 mm i.d., 0.25  $\mu\text{m}$  film thickness) was used. Column temperature was  $38 \text{ }^\circ\text{C}$  for  
194 1 min; it increased up to  $300 \text{ }^\circ\text{C}$  with ramping at  $6 \text{ }^\circ\text{C min}^{-1}$  and was held 5 min at  $300 \text{ }^\circ\text{C}$ . Samples  
195 were run in the electron impact mode at 70 eV and in the selected ion monitoring (SIM) mode with  
196 a 4.04 s scan time over a 50–450 amu range resolution. Each compound was recognized by a target  
197 ion and two qualifiers.

198  
199 **2.4.3 Water-soluble fraction of light crude oil dissolved in freshwater (WSF):** Adsorption  
200 experiment with crude oil dissolved in water was performed in order to evaluate the adsorption  
201 capacity of the MB3py550 toward a real complex matrix. Light crude oil, obtained from Rincon de  
202 los Sauces, Neuquen, Argentina, stored at  $4 \text{ }^\circ\text{C}$ , was used to prepare the WSF. A solution composed  
203 of crude oil ( $300 \text{ } \mu\text{g mL}^{-1}$  in methanol) and freshwater at a ratio of 1:100 (v/v) was stirred for 72 h  
204 at  $20 \text{ }^\circ\text{C}$  in the dark. WSF was separated using the bottom drain and was stored refrigerated at  $4 \text{ }^\circ\text{C}$   
205 for 24 h. In the adsorption experiment, 10 mg of MB3py550 were added to a 200 mL WSF sample  
206 and the mixture was placed on a magnetic shaker and allowed to equilibrate for 24 h at  $20^\circ\text{C}$ , in the  
207 dark. Then, the 150 mL of supernatant was magnetically separated and spiked with recovery  
208 standards (1-chloro-octadecane). Hydrocarbons concentrations in the supernatant, expressed as total

209 petroleum hydrocarbons (TPHs: C6-C35), diesel range (DRO: C10-C25) and residual range (ORO:  
210 >C25-C35) was determined by gas chromatography flame ionization detector (CG-FID) following  
211 the procedure described below: 150 mL of sample was eluted through Strata RP-18 cartridge using  
212 6 mL of hexane and 3 mL of dichloromethane. The fraction was concentrated to 1 mL under a  
213 nitrogen stream, transferred to a glass vial and quantified by GC-FID. An Agilent (Miami, USA),  
214 6890 gas chromatograph equipped with a ZB-5 fused silica capillary column (30 m × 0.25 mm i.d.,  
215 0.25 µm film thickness) and a flame ionization detector (FID) was used. Analyses were conducted  
216 in splitless mode using nitrogen as a carrier gas at a flow rate of 2 mL min<sup>-1</sup>. The column  
217 temperature was programmed from 60 °C to 300 °C at a rate of 6 °C min<sup>-1</sup> and held at 300 °C for 5  
218 min. Quality control and quality assurance protocols to ensure the accuracy and precision of  
219 analyses included: employing blanks and reference material and duplicate samples. The average  
220 recoveries based on matrix spiked samples were 70-110% and limit of detections are determined to  
221 be 13 µg L<sup>-1</sup> for TPHs and 17 µg L<sup>-1</sup> for PAH fraction.

222

223 **2.5 Regeneration and reuse of BBS-derived carbon magnet-sensitive materials:** Each cycle  
224 of reuse consisted of two stages: sorption and regeneration. For the sorption, 50 mg of MB3py550  
225 was contacted with 100 mL of 80 µg L<sup>-1</sup> ANT solution during 3 h. After magnetic separation, an  
226 aqueous aliquot was withdrawn for the determination of ANT equilibrium concentration and the  
227 remained supernatant was discarded. Later, for the regeneration stage, 10 mL of methanol was  
228 added to the MB3py550 and the dispersion was shaking for 10 min. The solid was magnetically  
229 separated and the regenerated MB3py550 was then reused for subsequent ANT sorption  
230 experiments again.

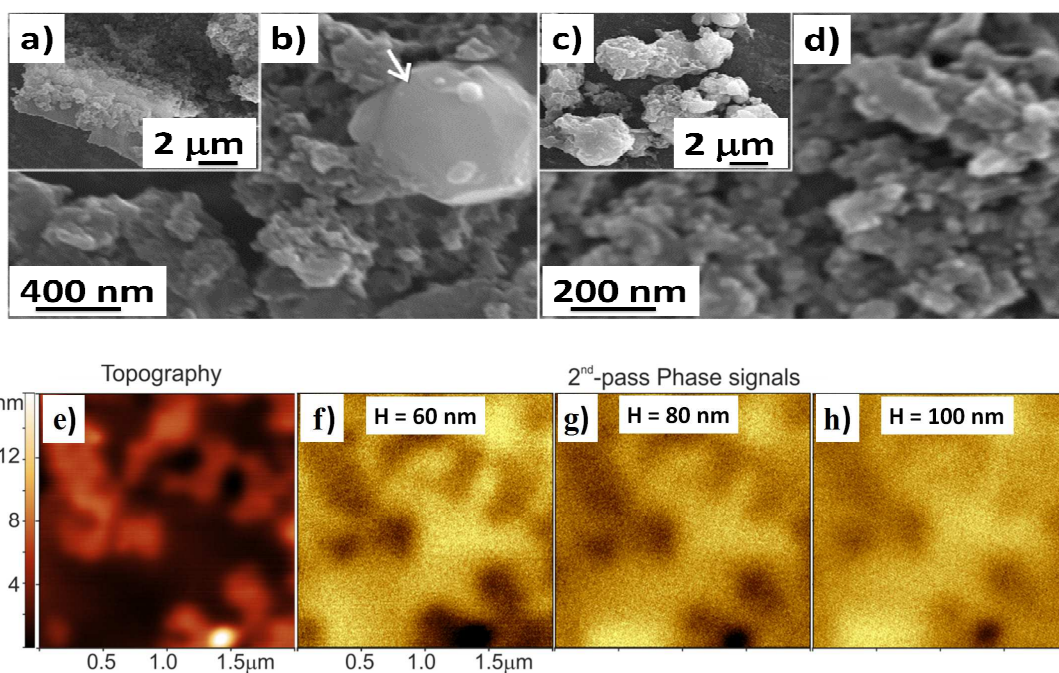
231

### 232 3. Results and discussion

#### 233 3.1 Morphological and magnetic characterization

234 Considering the results of the adsorption study reported below, the main part of the characterization  
235 studies described in the following concerns the sample showing the best performance in terms of  
236 pollutant removal, i.e. MB3py550 and its precursor MB3.

237 The morphology of the MB3 and MB3py550, are shown in **Figure 1a-d**. From the low-resolution  
238 SEM images (**Figure 1a,c**), it is clear that both samples are in the form of microagglomerates  
239 having irregular shape and exposing a complex surface. At higher magnification (**Figure 1b,d**),  
240 more evident aggregated nanoparticles with sizes in the 20-80 nm range (at the adopted resolution),  
241 are illustrated. From **Figure 1b**, it can be also noticed that salts or by-products (evidenced in the  
242 figure by the white arrow) can be present in the sample after water washing and drying, while a  
243 more homogeneous aspect is obtained for the thermally treated samples (**Figure 1d**).



258 **Figure 1.** Low- and high-resolution SEM images of both MB3 (a,b), and MB3py550 (c,d). The  
259 arrow in section b) evidences the presence of some synthesis by-product. AFM topography of  
260 MB3py550 (e), MFM phase shift images (f,g,h) of region e) obtained at various lift heights (H = 60  
261 nm, 80 nm and 100 nm, respectively).

262

263 Aggregated nanoparticles, 20-50 nm in sizes, are shown in the topography image of AFM/MFM  
264 (**Figure 1e**). Besides the AFM topography shown in **Figure 1e**, the phase shifting of the same  
265 region obtained in a second-pass lifted acquisition was operated at different heights ( $H = 60$  nm, 80  
266 nm, 100 nm) by using the same tip probe for analyzing the magnetic interactions and minimizing  
267 topographic effects. The intensity of the negative phase shifting, that is typically associated with the  
268 attractive interactions between the tip and the sample (dark regions in **Figure 1f-h**), was found to  
269 depend on the adopted heights: the higher resolution was obtained at  $H = 60$  nm and the magnetic  
270 characteristics of the more prominent nanoparticles were found at  $H = 80$  nm, while at higher  
271 heights the signal-to-noise ratio is minimized.

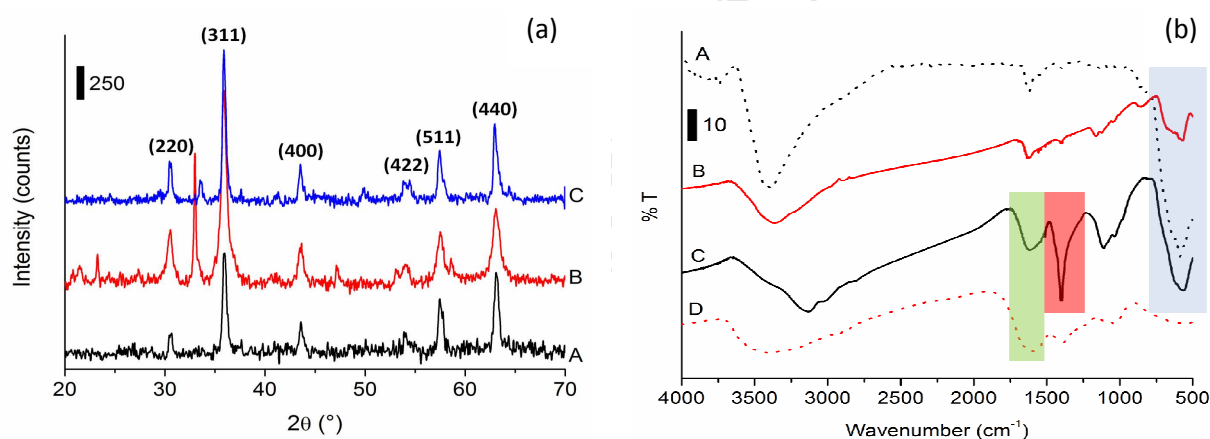
272 To better investigate the magnetic properties, an extensive characterization was performed. The  
273 magnetic properties of all samples are reported in **Table S2**, whereas magnetization curve profiles  
274 of both reference magnetite/maghemite and the MB3-series of samples are reported in **Figure S2**.  
275 In general, all bare samples (not thermally treated) reveal superparamagnetic behaviors, with  
276 negligible remanence ( $M_r$ ) and very low coercivity ( $H_c$  below 10 Oe). As already reported in our  
277 previous work (Franzoso et al., 2017), the values of saturation magnetization ( $M_s$ ) of bare BBS-  
278 stabilized NPs were respectively 56 (MB1), 36 (MB2), and 30 (MB3)  $\text{emu g}^{-1}$ , thus suggesting a  
279 different amount of magnetite/maghemite per gram of sample. Moreover, the decrease in terms of  
280  $M_s$  for all the BBS-stabilized samples compared to the neat magnetite M0 ( $64 \text{ emu g}^{-1}$ ) is mainly  
281 due to the presence of the BBS shell, which induces the reduction of the surface magnetic moments  
282 (Kim et al., 2003; Sun et al., 2009; Cesano et al., 2015; Bianco Prevot et al., 2017; Franzoso et al.,  
283 2017; Nisticò, 2017b).

284 Conversely, the pyrolysis treatment performed at  $550$  °C mainly affects the remanence (which  
285 moves from almost zero up to  $3.4\text{-}5.2 \text{ emu g}^{-1}$ ) and the coercivity (which increases from less than

286 10 up to 53-82 Oe). However, saturation magnetization value still remains below the neat  
 287 magnetite/maghemite M0 value.

### 288 289 3.2 Pyrolysis-induced effects on BBS-derived magnet-sensitive NPs

290 In order to unveil the chemistry behind the pyrolysis treatments, both XRD and FTIR analyses were  
 291 performed at different experimental conditions. In particular, the iron oxide phases forming the  
 292 magnet-responsive inorganic core of the NPs were identified through XRD. For the sake of brevity  
 293 only the MB3-series of samples are displayed in **Figure 2.a**.



305 **Figure 2.a.** XRD patterns of the neat magnetite M0 (A, solid black curve), MB3 (B, solid red  
 306 curve), and MB3py550 (C, solid blue curve). Main reflections due to magnetite phase are  
 307 highlighted. Non-labeled peaks refer to by-products signals. **b.** FTIR spectra in the 4000-500  $\text{cm}^{-1}$   
 308 range relative to neat magnetite M0 (A, dotted black curve), MB3py550 (B, solid red curve) MB3  
 309 (C, solid black curve) and BBS-GC (D, dotted red curve).

311 By considering the bare MB3 sample (**Figure 2.a**, diffractogram B), all the crystalline planes  
 312 highlighted in the figure at  $2\theta = 30.1^\circ$  (220),  $35.4^\circ$  (311),  $43.0^\circ$  (400),  $53.9^\circ$  (422)  $57.2^\circ$  (511), and  
 313  $62.6^\circ$  (440) are consistent with both magnetite (card number 00-019-0629 from ICDD Database)  
 314 and maghemite (card number 00-039-1346 from ICDD Database) (Cesano et al., 2015). No relevant

315 reflections are expected from BBS since its XRD pattern presents only one broad amorphous  
316 contribution centered at ca.  $2\theta = 25^\circ$  and few negligible signals due to its ash content (**Figure S3**).  
317 All the extra signals (not labeled) are consistent with the presence of by-products of the co-  
318 precipitation reaction carried out in ammonia aqueous solution, i.e., ammonium-containing salts as  
319 ammonium chloride (card number 01-073-0363 from ICDD Database) in analogy to our previous  
320 work (Nisticò et al., 2017). Pyrolysis treatments carried out at  $550^\circ\text{C}$  favored the  
321 abatement/disappearance of these ammonia-derived salts, maintaining the magnetite/maghemite  
322 crystalline phases (**Figure 2.a**, diffractogram C).

323 Pyrolysis-induced changes affecting the organic shell and its interaction with the magnetic core of  
324 the NPs were followed by means of FTIR analysis in the  $4000\text{-}500\text{ cm}^{-1}$  range. Infrared spectra of  
325 both reference magnetite (M0) and BBS, together with those of the MB3-series are collected in  
326 **Figure 2.b**.

327 The signals at  $575$  and  $620\text{ cm}^{-1}$  evidenced in M0, MB3 and MB3py500 are due to Fe-O stretching  
328 vibrations and consistent with the presence of iron oxides (**Figure 2.b**, blue box) (Cesano et al.,  
329 2015; Franzoso et al., 2017; Nisticò et al., 2017), whereas the presence of BBS in MB3 is  
330 confirmed by the presence of the signal at ca.  $1600\text{ cm}^{-1}$  due to BBS-carboxylate stretching mode  
331 (Bianco Prevot et al., 2017) (**Figure 2.b**, green box) and  $1110\text{ cm}^{-1}$  which can be assigned to C-O  
332 stretching vibration. The interaction between BBS and the iron oxide core of the NPs is confirmed  
333 by the presence of the very sharp band at  $1400\text{ cm}^{-1}$  which is an evidence of the direct interaction  
334 between BBS-carboxylate functionalities and the magnetite surface (i.e., carboxylate-iron bond  
335 stretching mode) (Ou et al., 2009), and by the shift of the absorption band assigned to C-O  
336 stretching mode attributable to the organic matter (mainly polysaccharides and other BBS-derived  
337 substances) adsorbed onto the iron oxide surface (**Figure 2.b**, red box). The thermal treatment  
338 carried out at  $550^\circ\text{C}$  (**Figure 2.b**, curve B) induced the significant reduction of all the infrared  
339 signals representative of the BBS-GC coating. On the other hand, the presence of the absorption



340 band at  $1620\text{ cm}^{-1}$  typical of the C=C stretching mode, suggesting the incipient conversion of the  
341 BBS into graphite-like materials. The iron oxide phase signals at  $575\text{ cm}^{-1}$  and  $620\text{ cm}^{-1}$  remained  
342 unaltered, confirming what already evidenced by XRD results.

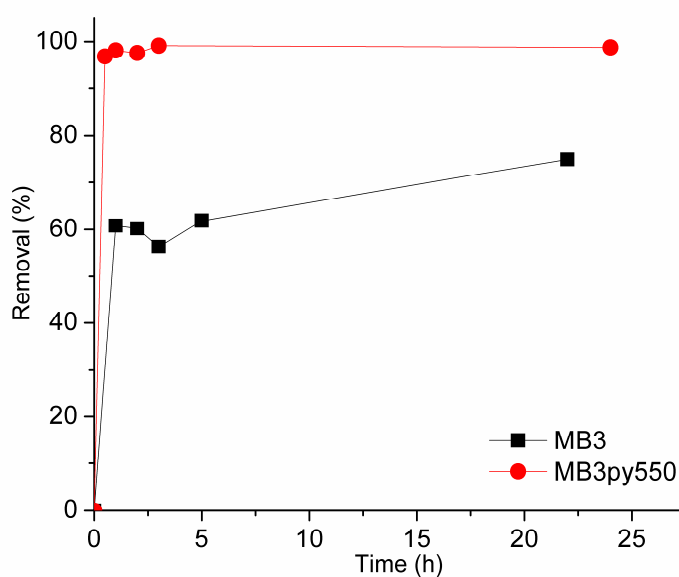
343 These characterization results of MB3py550 and its precursor MB3 were similar to those previously  
344 obtained in another synthesis batch (Nisticò et al., 2018), which confirms the reproducibility of the  
345 synthesis method.

346

### 347 **3.3 Adsorption studies**

348 Figure 3 shows the kinetic of adsorption of ANT toward both MB3 and MB3py550. The  
349 equilibrium was reached after approximately 3 h for MB3py550. Interestingly, MB3 showed some  
350 retention capacity toward ANT (70% of removal after 22 h of contact). This could be explained  
351 considering that ANT is capable of interacting with the  $\pi$  electrons associated with the aromatic  
352 moieties in the BBS matrix. However, a higher ANT % removal was obtained for MB3py550 (ca.  
353 99%), which is expected due to the increased hydrophobicity of the material after pyrolysis and  
354 consequent formation of graphite-like structures, thus confirming the results obtained from FTIR  
355 spectra. In all cases, pyrolyzed materials showed higher ANT uptake than non-pyrolyzed materials  
356 (data not shown). It is well documented in the literature that  $\pi$ -electron systems of the graphite-like  
357 materials can be engaged in  $\pi$ - $\pi$  electron-donor-acceptor (EDA) interactions with a series of  $\pi$ -  
358 donors (e.g., benzene, toluene, PAHs) which can enhance their removal capacity toward aromatic  
359 compounds (Zhu and Pignatello, 2005; Keiluweit and Kleber, 2009).

360



361

362

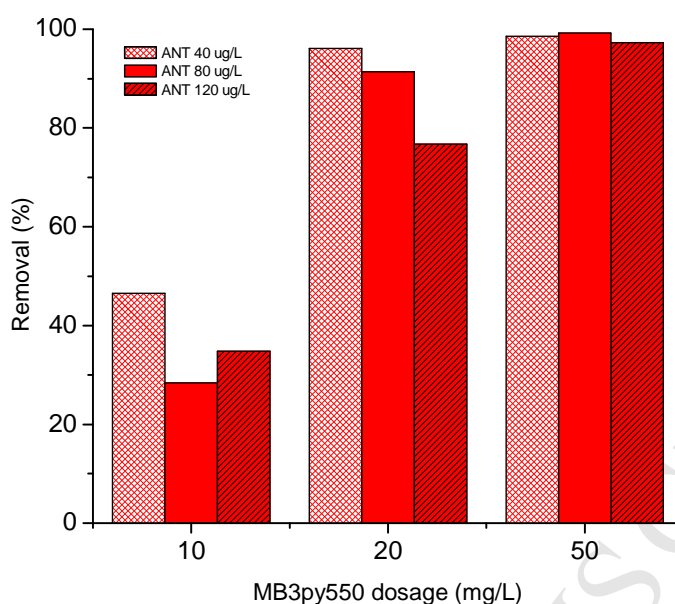
363 **Figure 3.** Kinetics of ANT adsorption on MB3 (black squares, black solid line) and MB3py550 (red  
 364 circles, red solid line) nanoparticles.  $[ANT]=50 \mu\text{g L}^{-1}$ ,  $[MB3py550]=500 \text{mg L}^{-1}$ .

365

366 The ANT removal capacity of the three pyrolyzed nanomaterials with different amounts of BBS-  
 367 GC (i.e. MB1py550, MB2 py550 and MB3 py550) was studied. The best uptake of ANT was  
 368 observed for MB3py550 (**Figure S4**), for this reason this adsorbent was selected for the  
 369 investigation of the potential application of these type of materials in different experimental  
 370 conditions.

371 In order to optimize the experimental conditions, and in particular to find out the minimum amount  
 372 of adsorbent needed for an effective ANT removal, sorption experiments were performed by  
 373 varying the amount of MB3py550 (10, 20 and  $50 \text{mg L}^{-1}$ ) for different ANT concentration ( $40, 80$   
 374 and  $120 \mu\text{g L}^{-1}$ ). The ANT removal capacity increased along with the adsorbent amount increase  
 375 achieving more than 95% removal for all ANT concentration tested with  $50 \text{mg L}^{-1}$  of MB3py550  
 376 and for  $40 \mu\text{g L}^{-1}$  ANT with  $20 \text{mg L}^{-1}$  of adsorbent (**Figure 4**).

377



378

379 **Figure 4.** Effect of initial concentration of ANT and [MB3py550] dosage on ANT removal.380 Contact time = 3 h. All experiments are performed at both  $20 \pm 1^\circ \text{C}$  and pH 6.

381

382 In order to compare our results with those reported in literature for different nanomaterials, the  
 383 sorption capacity of ANT, determined as the difference between initial concentration of ANT and  
 384 the equilibrium concentration of ANT per unit mass of adsorbent, was calculated for each  
 385 MBSS3py550 dosage and each initial ANT concentration tested in Figure 4. The highest sorption  
 386 capacity of ANT on MB3py550 was  $4.5 \text{ mg g}^{-1}$  corresponding to  $20 \text{ mg L}^{-1}$  of adsorbent dosage and  
 387 ANT concentration of  $40 \mu\text{g L}^{-1}$ . In terms of sorption capacity of ANT, MB3py550 is superior to  
 388 mesostructured silica nanoparticles ( $1.6 \text{ mg g}^{-1}$ ) (Topuz and Uyar, 2017), similar to electrospun  
 389 nanofibrous membranes ( $4.1 \text{ mg g}^{-1}$ ) (Dai et al., 2011) and lower than single-walled carbon  
 390 nanotubes multiwalled carbon nanotubes (Yang et al., 2006). However, being superparamagnetic,  
 391 the MB3py550 have the unique capability of being magnetically treatable. Moreover, a comparison  
 392 with previous results obtained with chitosan as a source of carbon for preparing carbon-coated  
 393 magnetic nanoparticles, shows that MB3py550 have a sorption capacity of ANT almost one order

394 of magnitude higher (Nisticò et al., 2017), which valorizes the use of BBS-GC in this type of  
 395 sorbents.

396 To evaluate the removal capacity of MB3py550 towards different PAHs, a mixture of NAP, ACL,  
 397 AC, FL, PHE, ANT, FN and PY was contacted with 50 mg L<sup>-1</sup> of adsorbent (**Figure 5.a**).

398

399

400

401

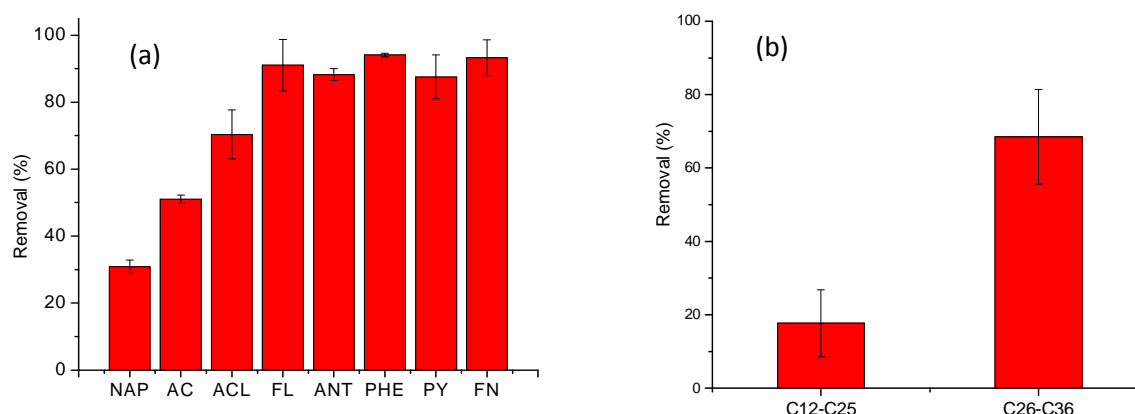
402

403

404

405

406



407 **Figure 5.a.** Adsorption experiments of PAHs on MB3py550. [PAHs] = 2.2 to 44 µg L<sup>-1</sup>,  
 408 [MB3py550] = 50 mg L<sup>-1</sup>, Contact time = 24 h. **b.** Uptake of the water-soluble fraction of crude oil  
 409 by MB3py550 nanoparticles. Conditions: [TPH] = 0.94 mg L<sup>-1</sup>, [MB3py550] = 50 mg L<sup>-1</sup>, Contact  
 410 time = 24 h. All experiments are performed at 20 ± 1 °C and pH 6. Error bars represent standard  
 411 deviation of three independent experiments.

412

413 The results show different removal capacities depending on the structure of PAHs; in particular,  
 414 high % removal (> 80%) was obtained for FL, ANT, PHE, PY and FN, whereas lower retention was  
 415 observed for NAP, AC and ACL. The removal capacity increased along with the number of  
 416 aromatic rings in the polycyclic structure and the PAHs hydrophobicity, suggesting that the  
 417 pyrolyzed nanomaterials are substantially good in the removal of PAHs from aqueous solutions.  
 418 Moreover, a clear trend of the removal capacity with the PAHs hydrophobicity ( $K_{ow}$ ) was also  
 419 observed (see  $K_{ow}$  values in the experimental section). These results can be explained considering  
 420 that the PAHs sorption occurs following two mechanisms: in the first one the  $\pi$ - $\pi$  interactions allow

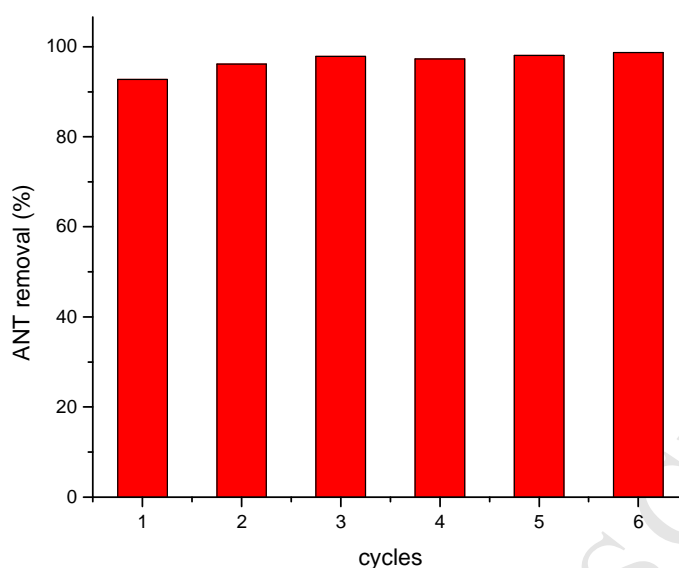
421 the adsorption of the molecules with the more extended aromaticity, whereas in the second one the  
422 hydrophobicity of the material attracts PAHs to the adsorbing surface.

423 Finally, the removal capacity of BBS-derived carbon magnet-sensitive adsorbent toward a sample  
424 water spiked with crude oil was studied. The experiment was performed by putting in contact the  
425 water-soluble fraction (WSF) with MB3py500 ( $50 \text{ mg L}^{-1}$ ) at pH 6 and  $20 \pm 1 \text{ }^\circ\text{C}$ . The composition  
426 of the WSF used in the experiments was: C12–C25 alkanes ( $0.78 \text{ mg L}^{-1}$ ) and C26–C36 alkanes  
427 ( $0.16 \text{ mg L}^{-1}$ ). It is worth mentioning that the PAHs present in the WSF sample belong to the C26-  
428 C36 fraction. **Figure 5.b** shows a higher uptake of heavier fraction hydrocarbons carried out by  
429 MB3py550 (ca. 70% removal), thus meaning that the adsorption capacity increased along with the  
430 hydrocarbon hydrophobicity as was also observed for the PAHs adsorption test. These promising  
431 results encourage the use of urban wastes as starting materials for the preparation of sustainable  
432 substrates to be successfully applied in the removal of hydrocarbons from contaminated waters.

433 The ANT removal during six continuous cycles of regeneration and reuse are shown in Figure 6. It  
434 was found that no loss of ANT adsorption capacity was observed on the regenerated MB3py550  
435 after six cycles. This reusability of the adsorbent is one of the most important features for their  
436 promising applications in environmental detoxification, specifically continuous flow-through  
437 systems could be designed for contaminated water treatments with high ANT removal efficiency.

438

439



440

441 Figure 6. Cycles of reuse (adsorption shown) of MB3py550 in the removal of ANT.  $[ANT]_0 = 80$   
442  $\mu\text{gL}^{-1}$ ,  $[\text{MB3py550}] = 500 \text{ mgL}^{-1}$ , contact time = 3h.

443

#### 444 4. Conclusions

445 Urban composted biowaste-derived substances with a lignin-like structure have proven to be an  
446 effective carbon-source for the production of easily-recoverable, low-cost carbon-coated magnet-  
447 sensitive NPs, produced through pyrolysis treatments performed in nitrogen at 550 °C. Adsorption  
448 experiments testing the removal of PAHs from contaminated water evidenced that the samples  
449 thermally treated are effective due to the  $\pi$ - $\pi$  conjugation between the PAHs and the  $\pi$ -electron  
450 system of the pyrolyzed material. The successful adsorption results suggest their possible  
451 application in wastewater remediation processes from PAHs-induced pollution.

452

#### 453 Acknowledgements

454 This work was realized with the financial support for academic interchange by the Marie  
455 Sklodowska-Curie Research and Innovation Staff Exchange project funded by the European

456 Commission H2020-MSCA-RISE-2014 within the framework of the research project Mat4treaT  
457 (Project number: 645551). Compagnia di San Paolo and University of Torino are gratefully  
458 acknowledged for funding Project Torino\_call2014\_L2\_126 through “Bando per il finanziamento  
459 di progetti di ricerca di Ateneo – anno 2014” (Project acronym: Microbusters). Polytechnic of  
460 Torino is gratefully acknowledged for funding project Starting Grant RTD (project number:  
461 54\_RSG17NIR01).

462 The authors are grateful to the Universidad Nacional del Comahue, Argentina, Project 04/I217 for  
463 the financial support. Additionally, authors would like to acknowledge Dr. Flavio R. Sives (La  
464 Plata, Argentina) for magnetization measurements.

465

#### 466 **References**

- 467 Avetta, P., Nisticò, R., Faga, M.G., D'Angelo, D., Boot, E.A., Lamberti, R., Martorana, S., Calza,  
468 P., Fabbri, D., Magnacca, G. 2014. Hernia-repair prosthetic devices functionalised with  
469 chitosan and ciprofloxacin coating: Controlled release and antibacterial activity. *J. Mater.*  
470 *Chem. B*, 2 (32), 5287-5294.
- 471 Bailey, S.E., Olin, T.J., Bricka, R.M., Adrian, D.D. 1999. A review of potentially low-cost sorbents  
472 for heavy metals. *Water Res.*, 33 (11), 2469-2479.
- 473 Bautista, M.E., Pérez, L., García, M.T., Cuadros, S., Marsal, A. 2015. Valorization of tannery  
474 wastes: Lipoamino acid surfactant mixtures from the protein fraction of process wastewater.  
475 *Chem. Eng. J.*, 262, 399-408.
- 476 Bianco Prevot, A., Baino, F., Fabbri, D., Franzoso, F., Magnacca, G., Nisticò, R., Arques, A. 2017.  
477 Urban biowaste-derived sensitizing materials for caffeine photodegradation. *Environ. Sci.*  
478 *Pollut. R.*, 24 (14), 12599-12607.
- 479 Cesano, F., Fenoglio, G., Carlos, L., Nisticò, R. 2015. One-step synthesis of magnetic chitosan  
480 polymer composite films. *Appl. Clay Sci.*, 345, 175-181.
- 481 Cesano, F., Rahman, M.M., Bardelli, F., Damin, A., Scarano, D. 2016. Magnetic Hybrid Carbon via  
482 Graphitization of Polystyrene-co-Divinylbenzene: Morphology, Structure and Adsorption  
483 Properties. *ChemistrySelect*, 1 (10), 2536-2541.

- 484 Cesano, F., Rahman, M.M., Bertarione, S., Vitillo, J.G., Scarano, D., Zecchina, A. 2012.  
485 Preparation and adsorption properties of activated porous carbons obtained using volatile  
486 zinc templating phases. *Carbon*, 50 (5), 2047-2051.
- 487 Choi, I.S., Cho, E.J., Moon, J.H., Bae, H.J. 2015a. Onion skin waste as a valorization resource for  
488 the by-products quercetin and biosugar. *Food Chem.*, 188, 537-542.
- 489 Choi, I.S., Kim, Y.G., Jung, J.K., Bae, H.J. 2015b. Soybean waste (okara) as a valorization biomass  
490 for the bioethanol production. *Energy*, 93 (2), 1742-1747.
- 491 Dai, Y., Niu, J., Yin, L., Xu, J., Xi, Y. 2011. Sorption of polycyclic aromatic hydrocarbons on  
492 electrospun nanofibrous membranes: Sorption kinetics and mechanism. *J. Hazard. Mater.*,  
493 192 (3), 1409-1417.
- 494 Dave, D., Ghaly, A.E. 2011. Remediation technologies for marine oil spills: A critical review and  
495 comparative analysis. *Am. J. Environ. Sci.*, 7 (5), 424-440.
- 496 Deng, J., You, Y., Sahajwalla, V., Joshi, R.K. 2016. Transforming waste into carbon-based  
497 nanomaterials. *Carbon*, 96, 105-115.
- 498 Fava, F., Totaro, G., Diels, L., Reis, M., Duarte, J., Carioca, O.B., Poggi-Varaldo, H.M., Ferreira,  
499 B.S. 2015. Biowaste biorefinery in Europe: Opportunities and research & development  
500 needs. *New Biotechnology*, 32 (1), 100-108.
- 501 Franzoso, F., Nisticò, R., Cesano, F., Corazzari, I., Turci, F., Scarano, D., Bianco Prevot, A.,  
502 Magnacca, G., Carlos, L., Mártire, D.O. 2017. Biowaste-derived substances as a tool for  
503 obtaining magnet-sensitive materials for environmental applications in wastewater  
504 treatments. *Chem. Eng. J.*, 310, 307-316.
- 505 Franzoso, F., Vaca-Garcia, C., Rouilly, A., Evon, P., Montoneri, E., Persico, P., Mendichi, R.,  
506 Nisticò, R., Francavilla, M. 2016. Extruded versus solvent cast blends of poly(vinyl alcohol-  
507 co-ethylene) and biopolymers isolated from municipal biowaste. *J. Appl. Polym. Sci.*, 133  
508 (9) pp. 43009.
- 509 Hao, W., Björkman, E., Yun, Y., Lilliestr, M., Hedin, N. 2014. Iron oxide nanoparticles embedded  
510 in activated carbons prepared from hydrothermally treated waste biomass. *ChemSusChem*, 7  
511 (3), 875-882.
- 512 Hu, H., Zhao, Z., Gogotsi, Y., Qiu, J. 2014. Compressible Carbon Nanotube-Graphene Hybrid  
513 Aerogels with Superhydrophobicity and Superoleophilicity for Oil Sorption. *Environ. Sci.*  
514 *Technol. Lett.*, 1 (3), 214-220.
- 515 Keiluweit, M., Kleber, M. 2009. Molecular-Level Interactions in Soils and Sediments: The Role of  
516 Aromatic  $\pi$ -Systems. *Environ. Sci. Technol.*, 43 (10), 3421-3429.



- 517 Kim, D.K., Mikhaylova, M., Zhang, Y., Muhammed, M. 2003. Protective coating of  
518 superparamagnetic iron oxide nanoparticles. *Chem. Mater.*, 15 (8), 1617-1627.
- 519 Lata, S., Samadder, S. Removal of arsenic from water using nano adsorbents and challenges: A  
520 review. *J. Environ. Sci.*, 166, 387-406.
- 521 Lee, J., Kim, J., Hyeon, T. 2006. Recent progress in the synthesis of porous carbon materials. *Adv.*  
522 *Mater.*, 18 (16), 2073-2094.
- 523 Li, Y., Yuan, D., Dong, M., Chai, Z., Fu, G. 2013. Facile and Green Synthesis of Core-Shell  
524 Structured Magnetic Chitosan Submicrospheres and Their Surface Functionalization.  
525 *Langmuir*, 29 (37), 11770-11778.
- 526 Lu, A.H., Salabas, E.L., Schüth, F. 2007. Magnetic nanoparticles: Synthesis, protection,  
527 functionalization, and application. *Angew. Chem. Int. Edit.*, 46 (8), 1222-1244.
- 528 Magnacca, G., Allera, A., Montoneri, E., Celi, L., Benito, D.E., Gagliardi, L.G., Gonzalez, M.C.,  
529 Mártire, D.O., Carlos, L. 2014. Novel Magnetite Nanoparticles Coated with Waste-Sourced  
530 Biobased Substances as Sustainable and Renewable Adsorbing Materials. *ACS Sustainable*  
531 *Chem. Eng.*, 2 (6), 1518-1524.
- 532 Magnacca, G., Laurenti, E., González, M.C., Arques, A., Prevot, A.B. 2015. Effect of humic  
533 substances and bioorganic substrates from urban wastes in nanostructured materials  
534 applications and synthesis. in: *Soluble Bio-based Substances Isolated from Urban Wastes.*  
535 *Environmental Applications*, (Eds.) A. Arques, A.B. Prevot, Springer International  
536 Publishing AG. Cham (Switzerland), pp. 41-58.
- 537 Magnacca, G.; Guerretta, F.; Vizintin, A.; Benzi, P.; Valsania, M.C.; Nisticò, R. 2018. Preparation,  
538 characterization and environmental/electrochemical energy storage testing of low-cost  
539 biochar from natural chitin obtained via pyrolysis at mild conditions. *Appl. Surf. Sci.*, 427,  
540 883-893.
- 541 Manna, L., Bugnone, C.A., Banchemo, M. 2015. Valorization of hazelnut, coffee and grape wastes  
542 through supercritical fluid extraction of triglycerides and polyphenols. *J. Supercrit. Fluid.*,  
543 104, 204-211.
- 544 Mehta, D., Mazumdar, S., Singh, S.K. 2015. Magnetic adsorbents for the treatment of  
545 water/wastewater-A review. *J. Water Process Eng.*, 7, 244-265.
- 546 Nardi, T., Sangermano, M., Leterrier, Y., Allia, P., Tiberto, P., Månson, J.A.E. 2013. UV-cured  
547 transparent magnetic polymer nanocomposites. *Polymer*, 54 (17), 4472-4479.
- 548 Nisticò, R., Barrasso, M., CarrilloLeRoux, G.A., Seckler, M.M., Sousa, W., Malandrino, M.,  
549 Magnacca, G. 2015. Biopolymers from Composted Biowaste as Stabilizers for the Synthesis

- 550 of Spherical and Homogeneously Sized Silver Nanoparticles for Textile Applications on  
551 Natural Fibers. *ChemPhysChem*, 16, 3902-3909.
- 552 Nisticò, R., Franzoso, F., Cesano, F., Scarano, D., Magnacca, G., Parolo, M.E., Carlos, L. 2017.  
553 Chitosan-Derived Iron Oxide Systems for Magnetically Guided and Efficient Water  
554 Purification Processes from Polycyclic Aromatic Hydrocarbons. *ACS Sustainable Chem.*  
555 *Eng.*, 5 (1), 793-801.
- 556 Nisticò, R., Celi, L., Prevot, A., Carlos, L., Magnacca, G., Zanzo, E., Martin, M. 2018. Sustainable  
557 magnet-responsive nanomaterials for the removal of arsenic from contaminated water. *J.*  
558 *Hazard. Mater.*, 342, 260-269.
- 559 Ou, X., Chen, S., Quan, X., Zhao, H. 2009. Photochemical activity and characterization of the  
560 complex of humic acids with iron(III). *J. Geochem. Explor.*, 102 (2), 49-55.
- 561 Pérez, C., Velando, A., Munilla, I., López-Alonso, M., Daniel, O. 2008. Monitoring polycyclic  
562 aromatic hydrocarbon pollution in the marine environment after the Prestige oil spill by  
563 means of seabird blood analysis. *Environ. Sci. Technol.*, 42 (3), 707-713.
- 564 Sun, X., Zheng, C., Zhang, F., Yang, Y., Wu, G., Yu, A., Guan, N. 2009. Size-controlled synthesis  
565 of magnetite (Fe<sub>3</sub>O<sub>4</sub>) nanoparticles coated with glucose and gluconic acid from a single  
566 Fe(III) precursor by a sucrose bifunctional hydrothermal method. *J. Phys. Chem. C*, 113  
567 (36), 16002-16008.
- 568 Teas, C., Kalligeros, S., Zanicos, F., Stournas, S., Lois, E., Anastopoulos, G. 2001. Investigation of  
569 the effectiveness of absorbent materials in oil spills clean up. *Desalination*, 140 (3), 259-  
570 264.
- 571 Topuz, F., Uyar, T. 2017. Cyclodextrin-functionalized mesostructured silica nanoparticles for  
572 removal of polycyclic aromatic hydrocarbons. *J. Colloid Interf. Sci.*, 497, 233-241.
- 573 Tran, V.S., Ngo, H.H., Guo, W., Zhang, J., Liang, S., Ton-That, C., Zhang, X. 2015. Typical low  
574 cost biosorbents for adsorptive removal of specific organic pollutants from water.  
575 *Bioresource Technol.*, 182, 353-363.
- 576 Vakili, M., Rafatullah, M., Salamatinia, B., Abdullah, A.Z., Ibrahim, M.H., Tan, K.B., Gholami, Z.,  
577 Amouzgar, P. 2014. Application of chitosan and its derivatives as adsorbents for dye  
578 removal from water and wastewater: A review. *Carbohydr. Polym.*, 113, 115-130.
- 579 Vane, C.H., Rawlins, B.G., Kim, A.W., Moss-Hayes, V., Kendrick, C.P., Leng, M.J. 2013.  
580 Sedimentary transport and fate of polycyclic aromatic hydrocarbons (PAH) from managed  
581 burning of moorland vegetation on a blanket peat, South Yorkshire, UK. *Sci. Total Environ.*,  
582 449, 81-94.

- 583 Wang, Z., Guo, H., Yu, Y., He, N. 2006. Synthesis and characterization of a novel magnetic carrier  
584 with its composition of Fe<sub>3</sub>O<sub>4</sub>/carbon using hydrothermal reaction. *J. Magn. Mater.*, 302  
585 (2), 397-404.
- 586 Yang, K., Zhu, L., & Xing, B. (2006). Adsorption of polycyclic aromatic hydrocarbons by carbon  
587 nanomaterials. *Environ. Sci. Technol.*, 40 (6), 1855–1861.
- 588 Zhao, H., Cui, H.J., Fu, M.L. 2016. A general and facile method for improving carbon coat on  
589 magnetic nanoparticles with a thickness control. *J. Colloid Interf. Sci.*, 461, 20-24.
- 590 Zhu, D., Pignatello, J.J. 2005. Characterization of Aromatic Compound Sorptive Interactions with  
591 Black Carbon (Charcoal) Assisted by Graphite as a Model. *Environ. Sci. Technol.*, 39 (7),  
592 2033-2041.
- 593
- 594
- 595

**Supplementary Material****From biowaste to magnet-responsive materials for water remediation from polycyclic aromatic hydrocarbons**

Roberto Nisticò<sup>a,b,‡</sup>, Federico Cesano<sup>a,c,‡</sup>, Flavia Franzoso<sup>a</sup>, Giuliana Magnacca<sup>a,c</sup>, Domenica Scarano<sup>a,c</sup>, Israel G. Funes<sup>d</sup>, Luciano Carlos<sup>e</sup>, Maria E. Parolo<sup>d,\*1</sup>.

<sup>a</sup> University of Torino, Department of Chemistry, Via P. Giuria 7, 10125 Torino, Italy.

<sup>b</sup> Polytechnic of Torino, Department of Applied Science and Technology DISAT, C.so Duca degli Abruzzi 24, 10129 Torino, Italy.

<sup>c</sup> NIS Interdepartment Centre, Via P. Giuria 7, 10125 Torino, Italy.

<sup>d</sup> Instituto de Investigación en Toxicología Ambiental y Agrobiotecnología, CITAAC (CONICET-UNCo), Facultad de Ingeniería, Universidad Nacional Del Comahue, Buenos Aires 1400, Neuquén, Argentina.

<sup>e</sup> Instituto de Investigación y Desarrollo en Ingeniería de Procesos, Biotecnología y Energías Alternativas, PROBIEN (CONICET-UNCo), Facultad de Ingeniería, Universidad Nacional Del Comahue, Buenos Aires 1400, Neuquén, Argentina.

<sup>‡</sup> Both authors contributed equally to this work.

**Table S1.** BBS-GC chemical composition and functional groups.

Metal analysis						
Si (%)	Fe (%)	Al (%)	Mg (%)	Ca (%)	K (%)	Na (%)
12.14±0.07	1.03±0.02	0.59±0.01	1.67±0.25	4.86±0.61	1.18±0.07	0.06±0.01
Microelements						
Cu (ppm)	Ni (ppm)	Zn (ppm)	Cr (ppm)	Pb (ppm)	Cd (ppm)	Hg (ppm)
73±1	100±3	157±13	49±1	43±2	<0.02	<0.02
General characteristics				Characteristics in aqueous solution 3g/L <sup>a)</sup>		
Moisture (%)	Ashes (%)	C (%)	N (%)	pH	Conducibility (μS/cm)	Surface tension (N/m)
3.69	31.2	39.94±0.35	4.82±0.14	9.02	429	56.8

Concentration values as mole fraction of total C for functional groups and C types in BBS-GC by

<sup>1</sup> \* Corresponding author. E-mail: maria.parolo@fain.uncoma.edu.ar, Ph.: +54 299 4490300 x 678, Fax: +54 299 4490329

NMR analysis<sup>b)</sup>

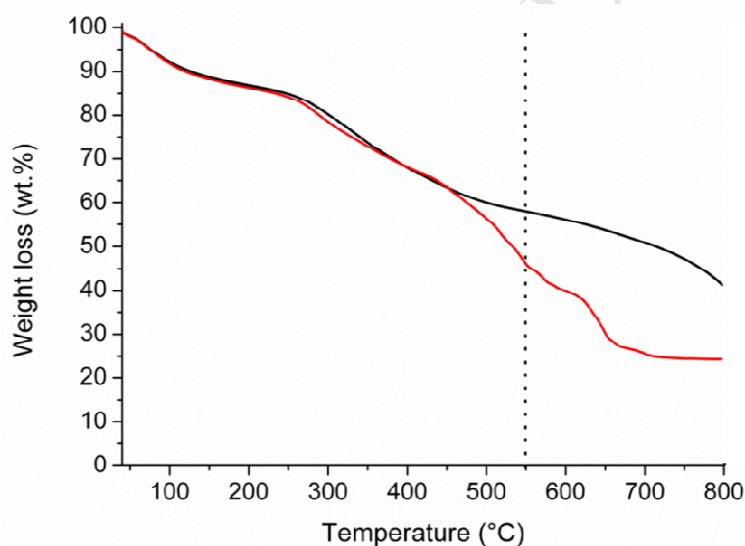
Aliph	NR	COOH	OR	Ph	PhOH	Kt
0.31	0.07	0.12	0.20	0.16	0.06	0.02

617 <sup>a)</sup> maximum solubility is 100 g/L in water at ca. 60 °C. solutions are stable in one week at different  
 618 temperatures (tests conducted at 4 °C, 25 °C and 40 °C) with water hardness  $\leq$  40 °F. <sup>b)</sup> legends: aliph =  
 619 aliphatic groups, NR = amino groups, COOH = carboxylic acids, OR = alkoxy groups, Ph = aromatic phenyl  
 620 groups, PhOH = phenoxy groups, Kt = ketones.

621

622 **BBS-GC thermal characterization**

623 Thermo-gravimetric analysis (TGA) was carried out by means of a TA Q600 (TA Instruments).  
 624 TGA tests were performed in order to monitor the BBS matrix degradation. The thermal analysis  
 625 was performed with a heating ramp of 10 °C/min from RT to 800 °C, either in nitrogen or in air  
 626 atmosphere. Two replicas were registered for each treatment condition.



627

628 **Figure S1.** TG curves of BBS-GC reference material heated either in nitrogen (solid black line) or  
 629 in air (solid red line) atmosphere. The black dotted line refers to the temperature investigated for the  
 630 pyrolysis treatments (namely, 550 °C).

631

632 The TGA analysis of BBS carried out in nitrogen (inert) atmosphere presents two main weight  
 633 losses: the first one due to the water evaporation (centered at ca. 100 °C), whereas the second one is  
 634 mainly due to the degradation phenomena involving the BBS organic structure (in the 250-600 °C  
 635 range). A carbonaceous residue (containing some ashes), which represented ca. the 50 wt.% of the  
 636 starting sample, was collected at 800 °C. Vice versa, the TGA analysis of BBS performed under air  
 637 (oxidant) atmosphere evidences the complete oxidation of the BBS organic shell, leaving an

638 inorganic residue, corresponding to the ash content in the sample, not far from the value of 31 wt.%  
 639 reported in **Table S1**.

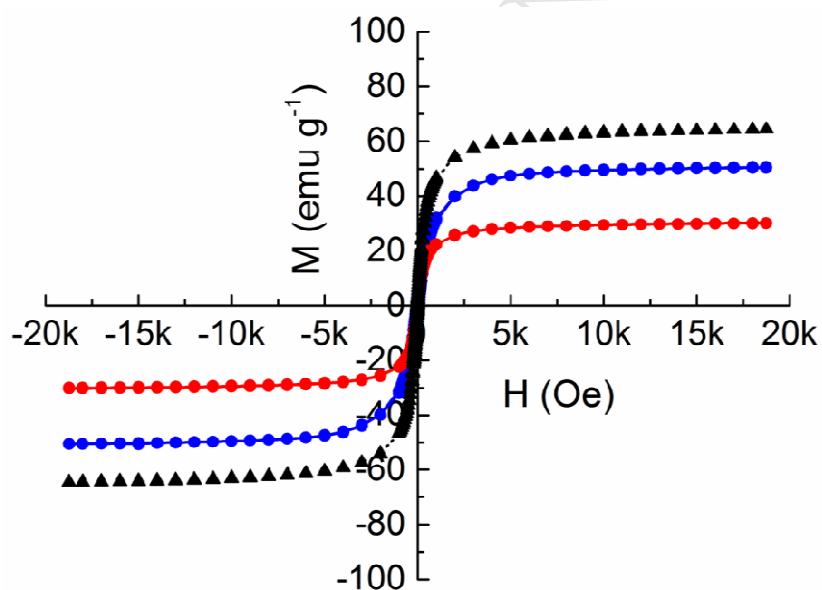
640

641 **Table S2.** Magnetic properties of samples registered at RT.

Samples	Saturation $M_s$ (emu/g)	Remanence $M_r$ (emu/g)	Coercivity $H_c$ (Oe)
M0	64	1.0	10
MB1	53	0.1	2
MB2	36	0.6	8
MB3	30	0.2	4
MB1py550	45	5.2	82
MB2py550	44	4.7	82
MB3py550	51	3.4	53

642

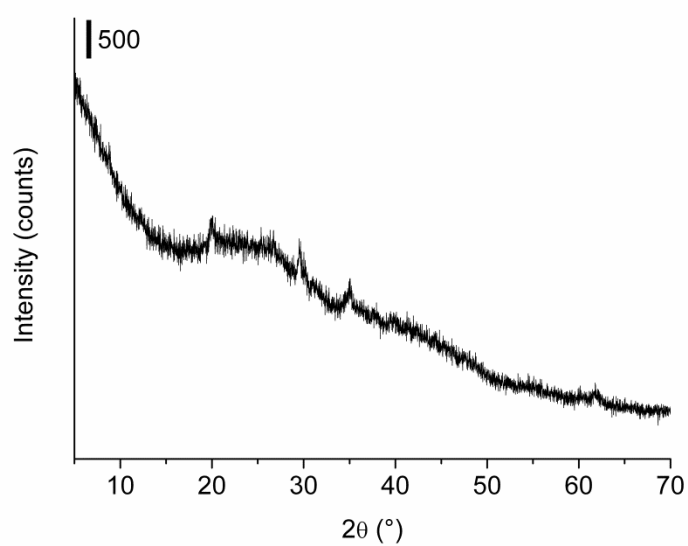
643



644

645 **Figure S2.** Magnetization curves relative to neat magnetite and BBS-stabilized (either as prepared  
 646 and pyrolyzed) samples. Legend: M0 (black triangles, dotted black curve), MB3 (red circles, solid  
 647 red curve), and MB3py550 (blue circles, solid blue curve).

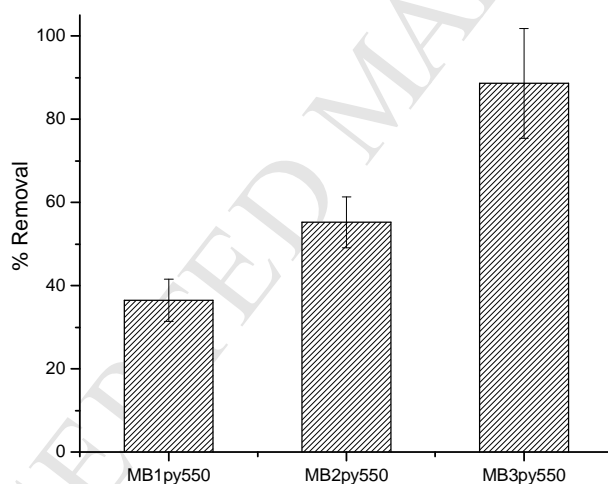
648



649

650 **Figure S3.** XRD pattern of the neat BBS-GC.

651



652

653 **Figure S4.** Effect of BBS-stabilized magnetite NPs used as adsorbent on ANT removal. [ANT] =  
654  $40 \mu\text{g L}^{-1}$ , [MBpy550] =  $20 \text{mg L}^{-1}$ , Contact time = 3 h. Error bars represent standard deviation of  
655 three independent experiments.

656

657

**HIGHLIGHTS**

- ~~Biowaste derived substances were used for production of magnet sensitive adsorbent.~~
- ~~Carbon coated magnetite NPs were produced through pyrolysis treatments.~~
- Biowaste-derived substances coated iron oxides are successfully used for PAHs removal.
- Thermally treated NPs show high adsorption capacity for PAHs.
- The reusability of NPs after six cycles is found to be excellent.
- Results encouraged the application of these NPs in wastewater remediation.